

Irradiation response of innovatively engineered metastable TRIP high entropy alloy

Priyanka Agrawal^{a,b}, Sanya Gupta^{a,b}, Abhijeet Dhal^{a,b}, Ramprashad Prabhakaran^c, Lin Shao^d, Rajiv S. Mishra^{a,b,*}

^a Center for Friction Stir Processing, Department of Materials Science and Engineering, University of North Texas, Denton, TX 76207, United States

^b Department of Materials Science and Engineering, University of North Texas, Denton, TX 76207, United States

^c Pacific Northwest National Laboratory, Richland, WA 99352, United States

^d Department of Nuclear Engineering, Texas A&M University, College Station, TX 77843, United States



ARTICLE INFO

Article history:

Received 6 October 2022

Revised 24 November 2022

Accepted 21 December 2022

Available online 22 December 2022

Keywords:

Irradiation resistance

High entropy alloys

Transformation induced plasticity

Self-healing

Transmission electron microscopy

Nanoindentation

ABSTRACT

Properties and radiation responses of a metastable high entropy alloy (HEA) exhibiting the transformation induced plasticity (TRIP) effect were studied. Innovative engineering used to manufacture this HEA has shown superior mechanical and corrosion properties in 3.5% NaCl than most advanced stainless steels. The microstructural evolution and corresponding mechanical response after irradiation have been evaluated using detailed transmission electron microscopy, and nanoindentation. The study shows a change in metastability of the alloy with irradiation via a recovery mechanism, where the irradiation-induced transformation is reversed by the temperature-induced transformation, thereby introducing the concept of self-healing, made possible due to the TRIP behavior of HEA.

© 2022 Elsevier B.V. All rights reserved.

1. Introduction

Nuclear energy is one of the environmentally and economically competitive clean energy options available today. To enhance the long-term viability and competitiveness of the existing fleet and to develop an advanced reactor pipeline, it is essential to develop and utilize innovative engineering methods and advanced materials for nuclear applications.

Irradiation leads to microstructural changes by introducing a range of defects that deteriorate the mechanical properties. The type and density of defects depend on various factors like the composition of the material, and initial microstructure, apart from severe in-service conditions experienced by the material like the irradiation dose, temperature, high stresses, and corrosive environment from the coolants used [1,2]. Irradiation leads to displacement cascades resulting in interstitials, vacancies, and line defects and their evolution with increasing dose leading to voids, dislocation loops, and dislocation networks that could also lead to phase

instabilities. The introduction of defects leads to radiation hardening, a low-temperature phenomenon, and ductility loss. If the irradiation is carried out at temperature and stress high enough to aid diffusion, the mobility of interstitials and vacancies can lead to irradiation creep, radiation induced segregation (RIS), radiation induced precipitation (RIP), and/or He-embrittlement. These defects evolve concomitantly affecting the mechanical, thermal, fatigue, creep, and corrosion properties [3].

Alloy design aims to reduce, if not avoid altogether, the detrimental defects that include their nucleation, migration, coalescence, and growth in these extreme service conditions. To develop radiation resistant materials for the next generation fission and fusion reactors, Zinkle and Snead [1,4] suggested basic design strategies: (i) straightforward and challenging route; to have a matrix that is inherently radiation resistant, (ii) to have the vacancies immobile at the service temperatures, or (iii) innovative engineering to increase sink densities for recombination of point defects. The current focus is on the alloy design strategy to fabricate an innovatively engineered material. Introducing a high density of centers for the recombination of point defects (high sink strength), have shown a reduced void swelling and RIS [1,5,6], following the kinetic rate theory. These centers can be dislocations, increased number of interfaces or nanostructure engineered alloy due to

* Corresponding author at: Center for Friction Stir Processing, Department of Materials Science and Engineering, University of North Texas, Denton, TX 76207, United States.

E-mail address: Rajiv.Mishra@unt.edu (R.S. Mishra).

thermo-mechanical treatments [7–11]. Zinkle et al. [4,6] showed the effect of 25% cold working on the remarkable improvement in void swelling resistance of austenitic stainless steel. A high density of precipitates or dispersoids was also reported to delay the swelling due to the creation of new interfaces, via engineered alloying additions and heat treatments [4,10,12].

For this study, an extensively explored metastable HEA was investigated for irradiation resistance that exhibits phase transformation due to deformation, the transformation induced plasticity (TRIP) effect, from FCC to HCP. In FCC systems, as stacking fault energy (SFE) decreases, the primary deformation mode is observed to change from slip (SFE > 40 mJ/m²), twinning induced plasticity (TWIP) (20 > SFE < 40 mJ/m²), or TRIP (SFE < 15 mJ/m²) [13]. Thus, a system with lower SFE activates the TRIP effect. Due to the high entropy of mixing, sluggish diffusion, severe lattice distortion, and cocktail effect; the core effects on which HEAs are designed [14–17]; the formation, growth/recombination, size, and the fraction of defects are expected to be different than conventionally used alloys for nuclear applications. HEAs are being considered for nuclear applications due to their promising mechanical properties and corrosion resistance. A limited number of studies have been performed to understand the irradiation behavior of HEAs. Although small in number, these studies suggest HEAs to be worth exploring for nuclear applications as they showed superior irradiation resistance as compared to conventional alloys [18–24] and the noteworthy observation was the absence of voids due to increased compositional complexity [18,25]. The past studies on irradiation effects were more focused on the quantification of radiation induced defects (fraction, size, and distribution), most of which were carried out at lower doses for single phase FCC (<50 dpa) [19,20,18,25] and BCC systems (<10 dpa) [23,26,27]. These studies also included the effect of the number of alloying elements by comparing a pure single element system with binary, ternary, quaternary, and quinary systems to explore the effect of multicomponent system [19,20,24] which is required for the generation of database to understand HEAs. There are only a handful of studies on single phase HEAs and a very limited number of studies on dual phase HEAs [28–30]. More importantly, the studies so far have not explored the TRIP effect of HEAs.

The current work is focused on proposing a *self-healing mechanism* by exploiting the TRIP effect in metastable HEAs and comparing the performance of the innovatively engineered alloy with materials currently used in nuclear applications via advanced microscopy, and nanoindentation studies.

2. Methods

2.1. Material

For the current study a metastable HEA Fe-20Mn-20Co-15Cr-5Si-1.5Cu (in at.%), referred to as Cu-HEA was used, which exhibits deformation-induced phase transformation from γ -fcc to ε -hcp, with stacking fault energy (SFE) reported to be <10 mJ/m² [31]. Cu addition led to a γ -fcc dominated alloy, which has shown to have excellent strength-ductility combination in different processing conditions (homogenized, rolled, friction stir processed), an exceptional fatigue resistance where the fatigue life improved due to the TRIP effect at the crack tip retarding the crack growth, and good corrosion resistance comparable to stainless steels [31–38]. This guided the choice of extensively studied Cu-HEA for this study to understand its irradiation behavior.

2.2. Innovatively engineered (IE) alloy

Cu-HEA was obtained from Sophisticated Alloys, Inc. (Butler, PA, USA), where the alloy was prepared via conventional induction

melting. The ingot with ~35 mm thickness was first homogenized (1100 °C) in the γ -fcc region for 2 h to obtain maximum γ -fcc and then rolled at 900 °C (γ -fcc domain) to a final thickness of ~6.5 mm, to get rid of the casting defects. The rolled sheet was then descaled and heated to 500 °C and then warm-rolled to a final thickness of ~3.15 mm. This innovative engineering technique led to a massively interfaced alloy, as shown in Fig. 1a.

2.3. Tensile and corrosion resistance as compared to nuclear materials

Tensile tests were carried out to understand the mechanical behavior of IE Cu-HEA at different temperatures (RT-650 °C). An in-house mini-tensile setup was used with 500 lbs. load cell capacity for the tensile tests at an initial strain rate of 10⁻³ s⁻¹. The subsized mini-tensile samples were machined using a CNC with ~5 mm gage length, ~1.2 mm thickness, and ~1.25 mm gage width, as per ASTM E8. The samples were ground to 4000 grit size and polished to 1 μ m surface finish using colloidal silica before testing, to avoid surface defects. The electrochemical corrosion experiments were carried out to understand the corrosion behavior as per ASTM F2129 and ASTM G61 in 3.5% NaCl solution at room temperature at a scan rate of 0.166 mV/s, with platinum as the reference electrode. The yield stress and corrosion resistance data were then compared, as shown in Fig. 1b and c, respectively with other nuclear materials.

As shown in Fig. 1b, an exceptionally high yield strength of ~1.2 GPa was achieved at room temperature with ~22% uniform ductility [39], placing this IE alloy in a high strength-ductility paradigm. An ultra-high strength was achieved via grain refinement and by introducing different types of interfaces: γ/γ , γ/ε , and ε/ε ; taking advantage of the TRIP behavior exhibited by this HEA to transform to ε -hcp from γ -fcc via plastic deformation. The IE Cu-HEA displayed superior performance than other nuclear materials at different temperatures, as seen from the comparison plot in Fig. 1b. A point to note is that MA957 TMT, which displayed similar behavior as the present alloy, is an oxide dispersion strengthened (ODS) ferritic alloy with a thermo-mechanical treatment (TMT) [40].

The high strength-ductility paradigm was achieved without sacrificing the corrosion resistance as compared to the initial condition, as reported in detail by Nene et al. [39,32]. From Tafel polarization curves (Fig. 1c), IE Cu-HEA is nobler as compared to heavily cold worked (CW) reference alloys used for nuclear applications. Irradiation experiments were planned after confirming the superior mechanical and corrosion properties of IE Cu-HEA.

2.4. Irradiation experiments

Samples of size 3 × 3 × 1 mm³ were machined using EDM (electrical discharge machining). A Multiprep™ polishing system (Allied High Tech Products, Inc.) was used for precision polishing, where all the samples were mounted together on the polishing fixture with a 3 × 3 mm² surface using crystal bond as the adhesive. The samples were then ground and polished to obtain a mirror finish with a final thickness, not more than 1 mm, to avoid a temperature gradient along the thickness from the beam exposure during the ion irradiation. The doses were determined using a Stopping and Range of Ions in Matter (SRIM) code under Kinchin-Pease (KP) mode as shown in Fig. 2. The irradiation experiments were performed using a 3.0 MV NEC tandem accelerator at Texas A&M University (TAMU). A static beam of 5 MeV Fe self-ions was used to avoid the pulse beam effect [52]. The irradiation temperatures selected were 350 and 500 °C, with peak damage levels ranging from 25 to 100 displacements-per-atom (dpa), representing the typical

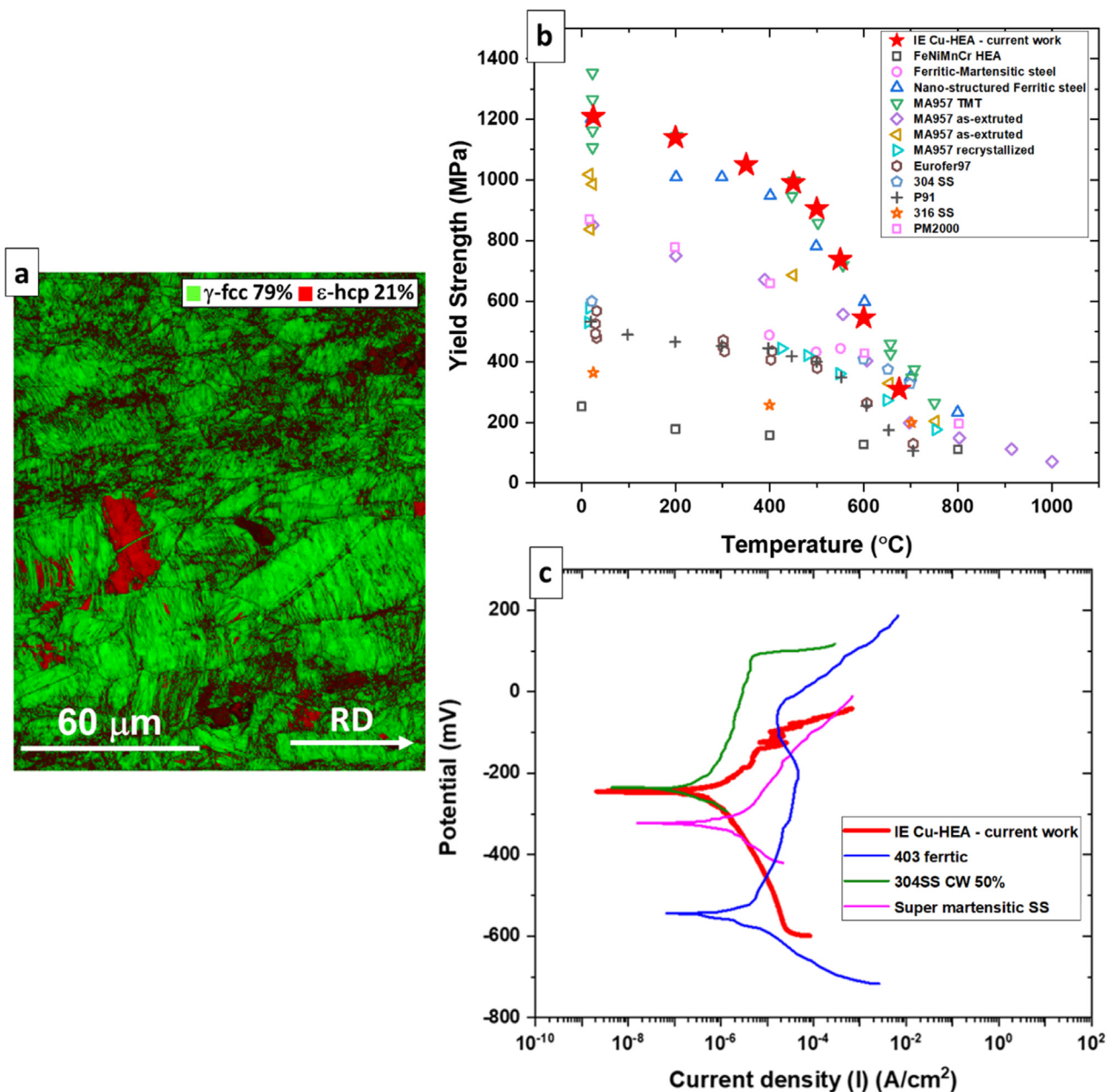


Fig. 1. (a) EBSD phase map with a massively interfacial microstructure with $\sim 79\%$ γ -fcc phase, (b) temperature dependent yield strength for different nuclear materials and compared with IE Cu-HEA (current work) [7,18,41–48], and (c) Tafel polarization plots for thermomechanically processed alloys used in nuclear plants, compared with IE Cu-HEA from current work [32,49–51].

Table 1
Ion irradiation parameters with 2E-3 as peak dpa rate for all irradiation.

Dose (dpa)	Ions/ cm^2	Irradiation Temperature (°C)	
25	2.43E+16	350	500
50	4.86E+16	350	500
100	9.72E+16	350	500

harsh environments in advanced reactors [53]. Furthermore, a multiple beam deflection technique was applied to avoid contamination [54]. Table 1 lists the key irradiation parameters including dpa, dpa rate, and temperature.

2.5. Microscopy

The as-received (AR) and irradiated IE Cu-HEA samples were characterized at the Microscopy Research Facility (MRF), University of North Texas (UNT), Denton. X-ray diffraction (XRD) was carried out to understand the phase evolution on self-ion irradiated samples. The Rigaku Ultima III high-resolution XRD was used with Cu- $\text{K}\alpha$ radiation operating at 40 kV and 44 mA across 35–100° 2θ range and a scan speed of 0.25°/min. Based on the XRD results, a few selected samples were taken for electron back-scattered diffraction (EBSD) study to identify γ/γ' interfaces to mill out samples for transmission electron microscopy (TEM). FEI Nova NanoSEM 230 equipped with a Hikari Super EBSD detector, was used to obtain the phase maps. TEM samples were milled using FEI Nova 200 NanoLab Dual Beam FIB/FESEM with Pt GIS, Omniprobe

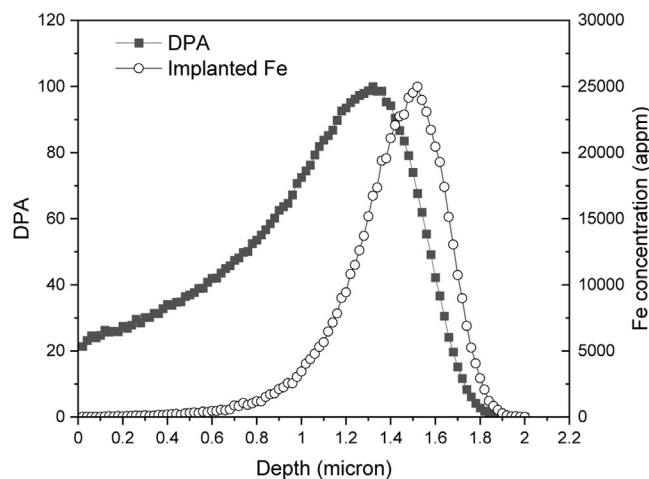


Fig. 2. SRIM simulation of IE Cu-HEA irradiated up to 100 peak dpa.

Nanomanipulator. The final steps of FIB milling included cleaning at 5 keV 41 pA and 15 pA and 2 keV 23 pA, to remove Ga ion damage at 30 keV. FEI Tecnai G2 F20 S-Twin 200 keV was used for traditional microscopy using diffraction contrast, compositional analysis in STEM mode using EDAX Octane T-Optima 30 mm detector, and TEM-based orientation image mapping (OIM) using precision electron diffraction (PED), to obtain the phase and orientation information at the nano-level. ASTAR hardware with TOPSPIN 3.1 software was used for the PED data acquisition, where ACOM 2.0 was used for analysis, all from NanoMEGAS.

2.6. Nanoindentation

Nanoindentation was carried out on AR and irradiated IE Cu-HEA samples at room temperature to evaluate irradiation hardening as a function of irradiation temperatures and doses. The experiments were carried out using the FemtoTools FT-NMT04 system using a Berkovich indenter in displacement-controlled mode till 150 nm depth to avoid interaction with the non-irradiated matrix [55]. A 5×5 array was used with a $25 \mu\text{m}$ spacing. The load-hold-unload cycle was 10–5–10 s with a velocity of $0.015 \mu\text{m s}^{-1}$.

3. Results and discussion

3.1. Phase evolution via XRD

Fig. 3 shows comparison plots of intensity vs. 2θ for as-received (AR) and irradiated IE Cu-HEA samples as a function of irradiation temperatures and doses. Fig. 3a shows the results obtained from samples irradiated at 350 °C. For AR, the peak $\sim 43.66^\circ 2\theta$ is identified as γ -fcc 111, $\sim 44.22^\circ$ as basal ε -hcp 0002 and $\sim 50.75^\circ$ as γ -fcc 200. This indicated the presence of γ -fcc and ε -hcp phases after IE in the AR sample. For the 25 dpa sample, there is not much difference compared to AR, except a marginal increase in ε -hcp 0002 peak and the start of the evolution of a phase around $\sim 44.85^\circ$, clearly seen in the overlapping plots (Fig. 3a₁). With a further increase in dose to 50 dpa there is a decrease in γ -fcc 111 and 200 peak intensity to nearly half, and now ε -hcp 0002 is one with the highest intensity. There is a clear evidence of the evolution of a new phase $\sim 44.85^\circ$ identified as σ -bct 002/200 peak. This follows the findings of Laplanche et al. [56,57] where kinetics and stability of σ -bct phase was reported in CrMnFeCoNi HEA. Further, Tsai et al. [58] and Liu et al. [59] had investigated the mechanical response change due to σ -bct phase formation in Al_{0.3}CrFeMnNi HEA. The γ -fcc 111 and 200 peaks at 50 dpa started showing asymmetry whereas γ -fcc 200 was observed to shift to a lower

2θ value. The reason for γ -fcc 111 asymmetric behavior could be due to the evolution of defects such as stacking faults, expected due to low SFE $<10 \text{ mJ/m}^2$ of the base alloy [60,61], or could be due to the evolution of a minor σ -bct phase peaks [56,57]. With 100 dpa irradiation the ε -hcp 0002 and σ -bct 002/200 peaks stood out but could not be deconvoluted even with a slower scan speed. There was a remarkable decrease in γ -fcc 111 peak intensity. γ -fcc 200 peak along with the reduced intensity showed a noticeable shift to a lower 2θ . At 350 °C, the lower irradiation temperature, with an increase in dpa, there was a remarkable decrease in γ -fcc 111, an increase in ε -hcp 0002 and a distinct evolution of σ -bct 002/200. Temperatures above 600 °C, in general, were shown to lead to σ -bct phase precipitation [62], but the increase in defect density has advanced the process to lower temperatures in the current work.

Fig. 3b presents the results obtained from samples irradiated at 500 °C. The observations at 25 dpa/500 °C were almost similar to the ones at 25 dpa/350 °C, except now ε -hcp 0002 was the dominating phase. The 50 dpa/500 °C specimen showed a deconvoluted peak for σ -bct phase and ε -hcp 0002 as the highest intensity peak and γ -fcc 111 peak intensity was slightly lower than AR or 25 dpa. Interesting results were seen for the 100 dpa specimen (with the highest dpa and irradiation temperature). The σ -bct 002/200 peak intensity increased with a new σ -bct peak ~ 40.96 and a new peak at ~ 48.42 which could be from σ -bct 331 or ε -hcp 1011. For 500 °C, unlike 350 °C, the γ -fcc 111 and 200 peaks showed a marginal decrease in intensity for 50 and 100 dpa. At 500 °C, with an increase in dpa, there was a marginal decrease in γ -fcc 111, with ε -hcp 0002 as the dominating peak and distinct evolution of σ -bct.

Based upon the XRD results, advanced microscopy was performed on a few selected samples in order to study the irradiation induced defects and metastability of the alloy.

3.2. Irradiation induced defects for IE TRIP HEA, imaged via TEM

As the XRD study provided distinct evidence for the presence of σ -bct phase in the higher combination of dpa and temperature, the extreme case of 100 dpa/500 °C was first studied to confirm radiation induced precipitation (RIP) via TEM. Fig. 4a is the low magnification image showing damage to an irradiation depth of $\sim 1.62 \mu\text{m}$ and it is in good agreement with the SRIM calculation. Irradiation resulted in a heterogeneous microstructure with the presence of dislocation loops and refined grain size. The dislocation loops were observed decorating the interface along [111]-fcc traces as shown in Fig. 4b. A similar observation was reported by Bawane et al. [63] for the presence of prismatic frank loops along {111} habit plane. Along with the observation of dislocation loops, precipitate-like features were also observed as seen in Fig. 4c. The features were confirmed to be σ -bct, using diffraction contrast as seen in Fig. 4d along with the diffraction pattern as the inset. For comparison, images were captured for the same dose, 100 dpa at 350 °C, Fig. 4e and f, where the microstructure remained heterogeneous with refined grains but with finer features of dislocation loops or precipitates. The complex microstructure due to IE and high dose levels makes it difficult to separate different features and quantify them. Further detailed TEM using diffraction contrast along with APT is ongoing to confirm the respective features, their size and fraction. Loop structures at high doses can evolve as networks that rearrange in the presence of temperature, leading to recrystallization [40,64], as seen for higher doses of 100 dpa in the present case.

Fig. 5 shows images of the other extreme condition with the lowest dose of 25 dpa at 500 °C and 350 °C. A clear decrease in feature size was observed from interface to surface for 25 dpa with no evidence of the formation of refined grains for this lower dose. Fig. 5a-c present images for 500 °C, where Fig. 5b is a micrograph

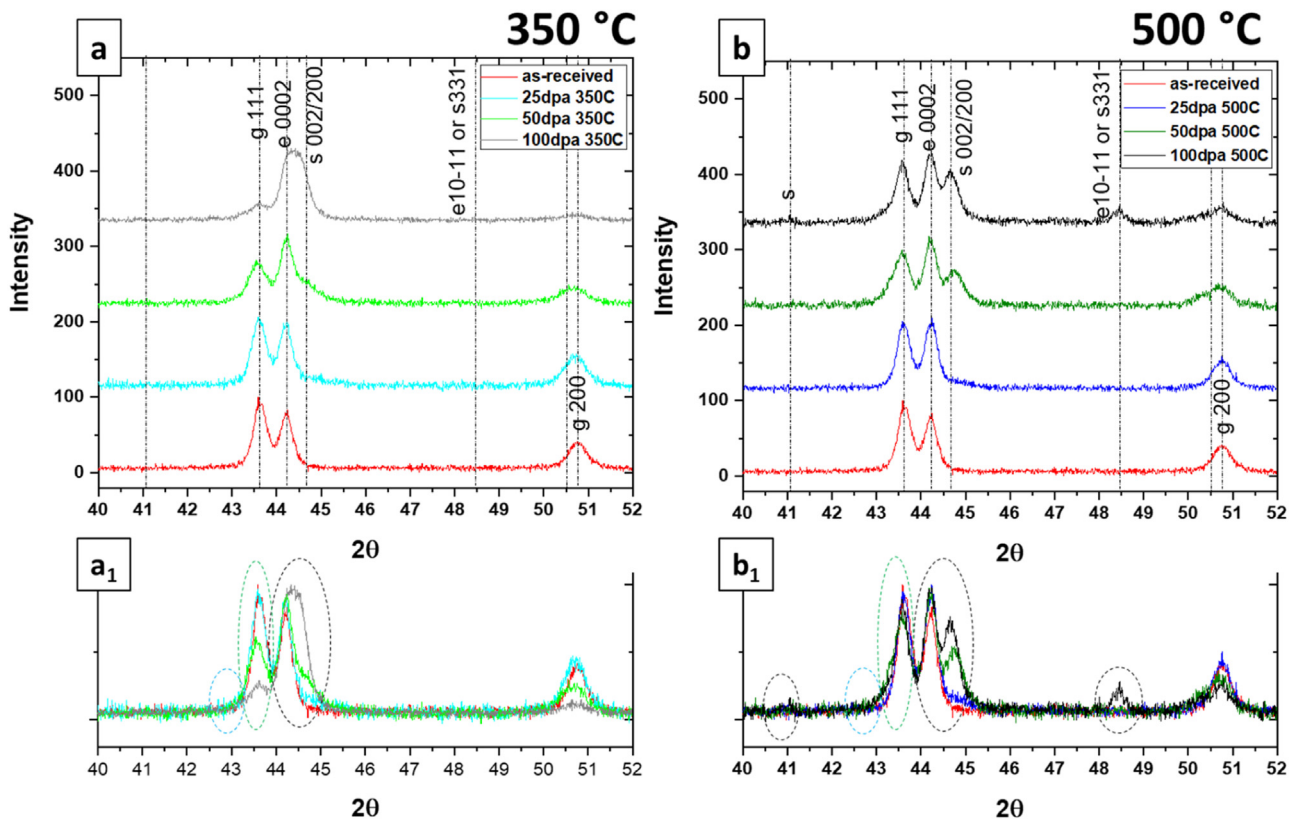


Fig. 3. Intensity vs. 2θ plots for AR and irradiated IE Cu-HEA samples with different doses (a) 350 °C and (b) 500 °C.

near the interface, with a higher loop/precipitate size, and Fig. 5c is near the surface with finer loops/precipitates. For 350 °C, a stitched and higher magnification image of Fig. 5d is shown in Fig. 5e to image the gradient in size of defects from the interface to the surface.

Further STEM-EDS was carried out for critical samples to look for radiation induced elemental partitioning (RIEP)/segregation (RIS). Fig. 6 gives elemental maps for Cr, Si, and Fe; where Cr and Si are σ -bcc stabilizers and Fe, the γ -fcc stabilizer, is the matrix. The yellow dash line in the EDS maps demarcates the irradiated region from the non-irradiated region, confirmed via TEM images using diffraction contrast. RIEP was observed in 100 dpa/500 °C sample, whereas 50 dpa/500 °C and 100 dpa/350 °C (lowest temperature and highest dosage) samples did not indicate the same. There is no evidence of RIS for the entire range of doses and temperatures.

Thus, RIP was observed for the entire range as captured by XRD, but RIEP was observed only at 100 dpa/500 °C. An important observation is that no voids are observed for the entire matrix of dose and temperature, following methods to characterize radiation damage by TEM [64], suggesting that **the current IE TRIP HEA is resistant to void formation and thus swelling**. One of the strategies to improve radiation resistance is to increase the sink density for the defects created during irradiation [7,65]. The absence of voids in this alloy is due to the large density of interfaces due to the IE technique [66]. Also, the current alloy is HEA where the absence of voids is reasoned due to the increased compositional complexity [18,20–22,53,67], where the high lattice distortion and sluggish diffusion reduce the point defect combination kinetics in HEAs [1,68,69]. Literature reports that the void swelling resistance depends on the number and type of alloying elements [20,70,71]. Work by Jin et al. [20] showed that the resistance for FeCoCrMn alloy with Ni is 40 times higher than pure Ni, where Fe and Mn

show a stronger influence on increasing the swelling resistance. Fig. 7 gives the plot of temperature and dose in-service conditions for different reactors superimposed with the domain of void swelling observed in various stainless steels and the experimental domain of current alloy with no voids/void swelling and experiencing a change in metastability with irradiation.

3.3. TRIP effect – Self-healing mechanism

To understand the metastability of the alloy and thus the underlying operative mechanism, 50 dpa/500 °C was chosen since its microstructure is a simpler one to study and easier to image using PED due to the absence of refined grains or RIEP and the presence of bigger dislocation loops due to the dpa/temperature combination, as shown in Fig. 8a. PED was carried out on Tecnai F20 in nano-probe mode using 8 spot size (~2 nm probe size), step size of 5 nm, and C2 aperture of 30 μm . Fig. 8b is the low magnification virtual dark field (VDF) where the region highlighted in the yellow box is taken for the PED scan. Fig. 8c gives a VDF, orientation image map (OIM), and phase map. The phase map in Fig. 8c₃ shows the matrix as γ -fcc in green and loops as ε -hcp in red. Fig. 8c₄ gives the misorientation information for the loops marked as A, B, and C, confirming the evolution of ε -hcp from γ -fcc. These are **faulted prismatic loops that transformed to ε -hcp due to the TRIP effect**, shown as schematic in Fig. 8d. This leads to a proposal of a self-healing mechanism, as shown in Fig. 9a, and thus an irradiation resistant material by exploiting the TRIP effect of the metastable HEA. Irradiation leads to a cascading effect, inducing deformation and thus transformation to ε -hcp via TRIP effect. With increasing temperature, there is a recovery mechanism, reversing the TRIP effect and thus self-healing the alloy from radiation damage. The concept is evidenced by considering XRD results for AR, 100 dpa/350 °C and 100 dpa/500 °C

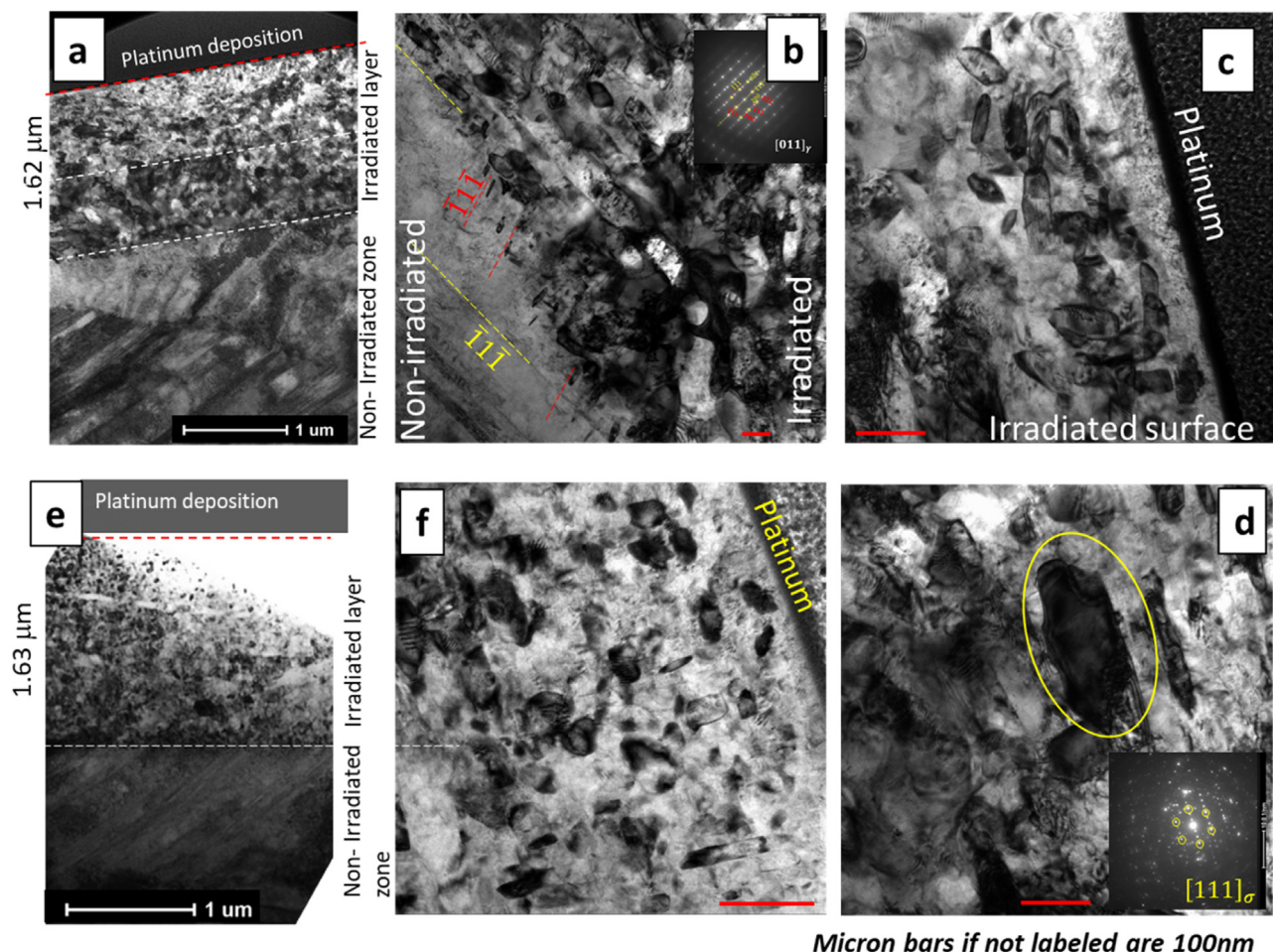


Fig. 4. Micrographs at 100 dpa and different temperatures. **500 °C:** (a) low magnification image with irradiated layer, (b) irradiated/non-irradiated interface decorated with dislocation loops along {111} fcc interfaces. Also observed are refined grains in the irradiated layer leading to a heterogeneous microstructure (inset is with diffraction pattern of [011] fcc zone axis), (c) high magnification micrograph near the surface imaging precipitate-like features along with dislocation loops, (d) confirmation of the features to be σ -bct precipitates at [111] zone axis. **350 °C:** (e) low magnification image, and (f) high magnification micrograph imaging finer features - dislocation loops and precipitates than one imaged at 500 °C as shown in (c). Note: Micron bars if not labeled are 100 nm.

samples, presented in Fig. 9b, and confirmation from TEM (Fig. 8). As compared to AR, the γ -fcc decreases and ε -hcp dominates with irradiation at the lower temperature of 350 °C, suggesting the TRIP effect and transformation of γ -fcc \rightarrow ε -hcp. With the increase in temperature to 500 °C, which is above the ε -hcp \rightarrow γ -fcc transformation temperature [73,74], recovery and thus reversal to γ -fcc takes place, suggested by an increase in 111 and 200 γ -fcc peaks at 100 dpa/500 °C. There are also loops where the TRIP effect is observed only at the interface, as marked in Fig. 8c₁ and c₃. These could be the shear loops where segregation might have occurred at the dislocations [21]. An important point to note here is that in the literature for the irradiation of HEAs, the lowering of point defects due to the core effects is termed as 'self-healing' [67] whereas the current work is focused on reversing the irradiation-induced transformation by temperature-induced transformation and thus minimizing degradation due to irradiation.

3.4. Mechanical response of irradiated samples

Nanoindentation was performed to understand the mechanical response of the alloy to irradiation as shown in Fig. 10a, where average hardness values are given for different irradiation conditions obtained from steady state regime of hardness vs. depth plots. In general, radiation increases hardness due creation of defects, termed radiation hardening [75]. The defect density keeps on

increasing with the increase in dpa. On the contrary, the hardness shows a decreasing trend with an increase in temperature for the same dpa level. This is because with the increase in temperature, the annihilation of defects and coarsening of remaining defects results in a decrease in defect density, thus decreasing hardness. For the present case, when the AR sample is compared with samples irradiated at 350 °C, Fig. 10a, a decrease in hardness is observed till 50 dpa, and a further steep rise is observed for 100 dpa, higher than the AR sample. Fig. 10b gives the TEM image for 50dpa/350 °C which displays minimum hardness. The hardness trends are reasoned on the basis of the microstructural evolution; observed and evaluated via microscopy in the previous sections. The basis to understand the trend is demonstrated as a schematic in Fig. 10c. Due to the TRIP effect, the irradiated sample has ε -hcp as the faulted prismatic loops. Thus, with an increase in γ -fcc phase fraction, there will be an increase in loop density due to irradiation – prismatic and shear loops and thus an increase in the fraction of ε -hcp phase, γ/γ and γ/ε interfaces.

It is important to note that the alloy for the current study is IE to have high sink densities. One of the reasons for the decrease of hardness for 25 and 50 dpa at 350 °C (Fig. 10a-d) is the annihilation of the defects at the sinks. As seen from XRD results (Fig. 10e), there is a drastic decrease in γ -fcc 111 intensity, making ε -hcp (0002 peak) the dominating phase for 50 dpa. However, it is expected that the hcp phase should increase the hardness. In

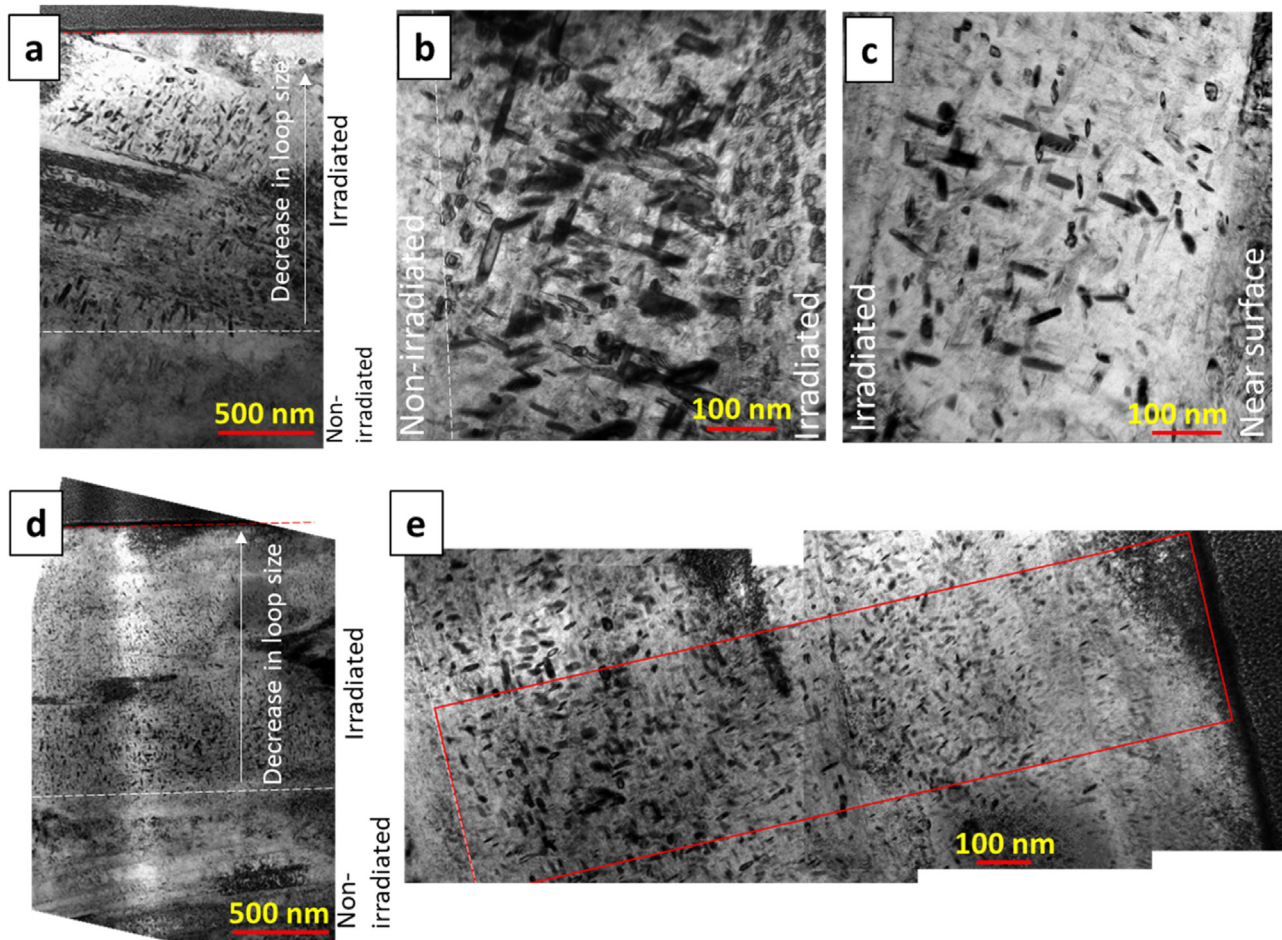


Fig. 5. TEM images for samples irradiated at 25 dpa and different temperatures. **500 °C:** (a) low magnification image. High magnification micrograph imaging loops/precipitates at the interface in (b) and the surface in (c) **350 °C:** (d) low magnification image, (e) high magnification stitched imaged to show the change in defect size with the irradiation depth.

In the present case, as seen from PED results the dislocation loop or the faulted region inside the loop transforms to ε -hcp due to the TRIP effect (Fig. 8). The dislocation loop fraction and loop size increase with the increase in the dose (in Figs. 4 and 5). Thus, with a decrease in γ -fcc phase fraction as seen from XRD, the dislocation loops density overall decreases, decreasing the γ/ε interfaces, thus decreasing the hardness (Fig. 10a,b,d). With 100 dpa the defect density is high enough, leading to a steep increase in hardness due to RIEP and RIP of σ -bct phase and increasing the interfaces due to refinement of grain size.

Hardness increases with an increase in temperature for a constant dose, unlike observed and reported in the literature for conventional alloys. With the increase in temperature, the γ -fcc phase fraction increases, leading to increased faulted and shear loops and thus increased γ/γ and γ/ε interfaces. For 500 °C, with an increased dose, the hardness increased (Fig. 10a and f). As compared to AR, the hardness of 25 dpa decreases as ε -hcp is evolving as the dominating phase as seen from XRD, although the increase is marginal (Fig. 10e). With 50 dpa, nothing much changes as seen from XRD plots, but dislocation loops size seems to be larger for 50dpa as compared to 25dpa, leading to increased interface fraction and thus increased ε -hcp fraction not captured by XRD. With a further increase in dpa to 100, there is refinement due to rearrangement. Thus, we see the highest hardness for 100 dpa/500 °C.

The average hardness plot shows that the error bars increase with the increase in dose for a constant temperature and increase with an increase in temperature for a constant dose. This shows

that the sample is becoming more heterogeneous with increased dose and temperature. An example is to compare error bars for AR specimen with 100 dpa dose at 350 °C and 500 °C. This observation supports the microstructural observation at the TEM level.

3.5. Guidance for metastability engineered alloys for minimizing irradiation damage

The current work merged all the three alloy strategies summarized by Zinkle and Snead [1]: (i) to have a material that is resistant to irradiation damage at operating temperatures or exhibits transformation and reverse transformation, **self-healing**, (ii) to have immobile vacancies; HEAs have proved to be an excellent candidate as no voids were observed as reported in the literature (Fig. 7) and the present case, (iii) innovative engineering was implemented to have sinks to allow the recombination of the point defects. During service, the self-healing mechanism will aid in minimizing the degradation due to irradiation as the TRIP effect will transform γ -fcc to ε -hcp, whereas the service temperature will lead to reverse transformation due to recovery. Microscopy along with nanoindentation gives a wholesome idea about the current alloy as a candidate for nuclear application with the innovative self-healing mechanism. With the primary hypothesis of the self-healing mechanism being validated, below are some remarks for the expansion of this concept and alloy design:

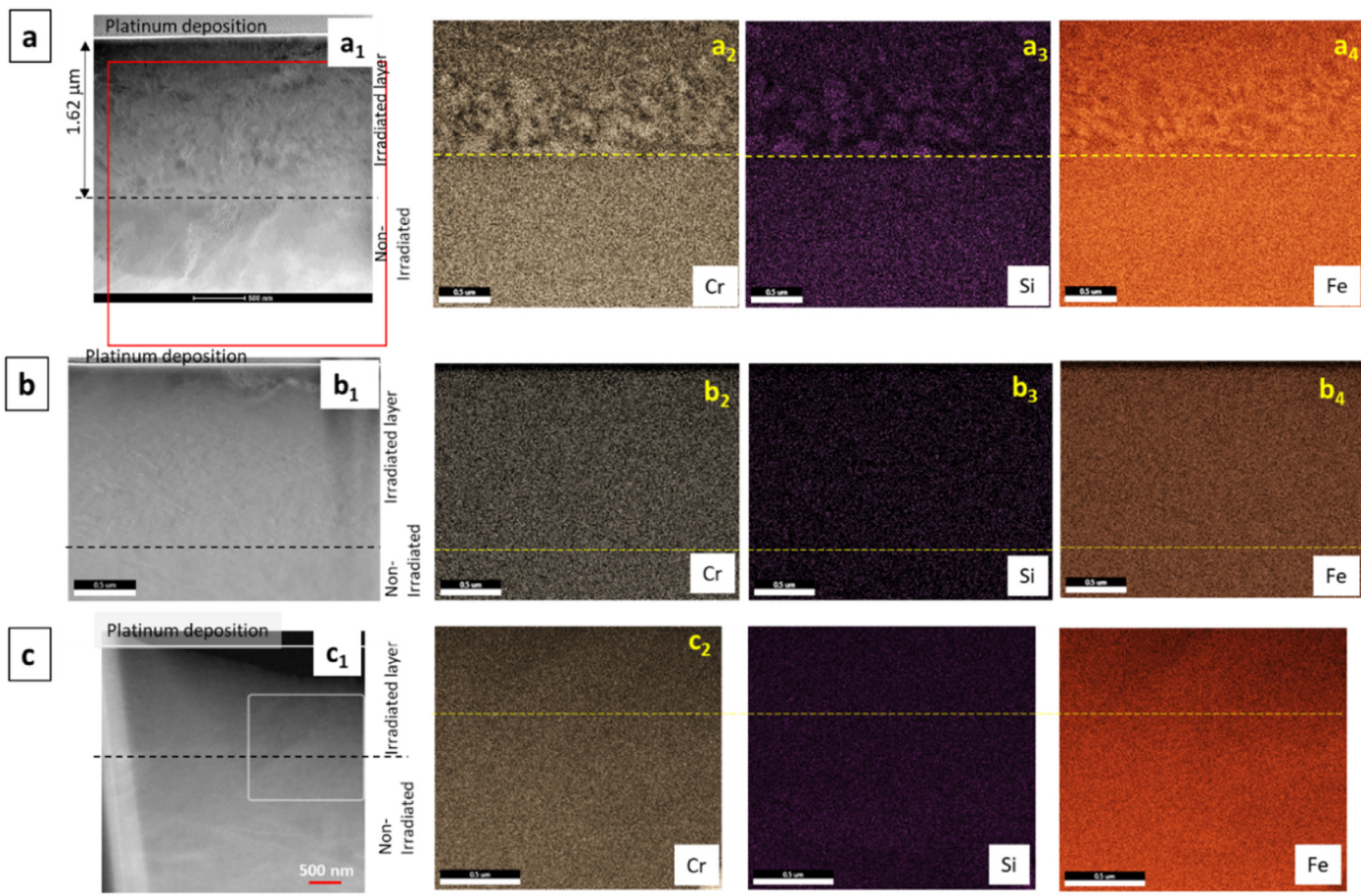


Fig. 6. STEM-EDS to investigate RIEP/RIS with Cr, Si, and Fe composition maps a) 100 dpa/500 °C, b) 50 dpa/500 °C, and (c) 100 dpa/350 °C. Note: All scale bars are 500 nm.

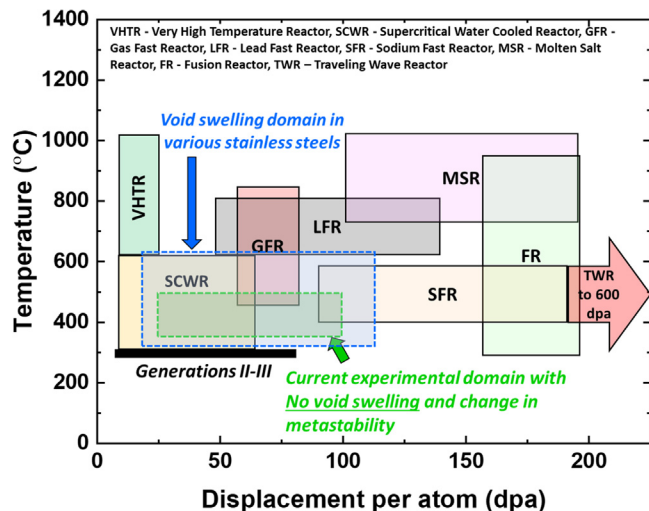


Fig. 7. The plot providing the temperature and dose in-service conditions for in-core structural materials for Gen IV reactors along with TWR and FR [53,72]. Superimposed is the range for void swelling domain observed in various stainless steels currently in use and the experimental domain for the current study that showed no void swelling and radiation induced metastability. (Figure adapted from S.J. Zinkle and G.S. Was, *Acta Materialia* 61 (2013) 735–758).

3.5.1. Expansion to other TRIP HEAs

The basic and simplest way suggested [1,4] to have a radiation resistant material is to have an inherently irradiation resistant matrix/phases. Ferritic-Martensitic steels with BCC as matrix

have better radiation resistance than austenitic stainless steels with FCC matrix. FCC is reported to have a higher defect density as compared to BCC for the same irradiation parameters [76], resulting in a better void swelling resistance of BCC when irradiated at higher temperatures [76]. However, from the recent review, the superior performance of BCC is reported to be still not fully understood [23]. BCC having more glissile defects, higher diffusivity due to open structure, and lower dislocation bias (preference to absorb interstitials as compared to vacancies by dislocations) due to a higher fraction of screw dislocations as compared to FCC, enhances recovery due to defect recombination and thus delays/suppresses the damage accumulation due to radiation [1,77].

In the current work, we explore the TRIP effect in γ -fcc dominated HEA with $<10 \text{ mJ/m}^2$ SFE, leading to transformation to HCP due to plastic deformation. HCP materials leads to grain boundary cracking due to anisotropic strains, thus not considered for nuclear applications [23]. But this study can be expanded to explore other metastability engineered TRIP HEAs for nuclear applications, FCC-BCC transformations, or better to explore BCC-FCC, where ferritic stainless steels are preferred as the matrix for nuclear applications using the self-healing concept. Due to the self-healing concept, the current dose and temperature envelope can be positively shifted to higher values for the TRIP alloys and can be considered for future fusion reactors (Fig. 7).

3.5.2. Alloy design to avoid σ -bct formation and have a Co-free alloy

In the present alloy, σ -bct phase was distinctly observed for 100 dpa at both irradiation temperatures. Cr-rich precipitates were only observed after irradiation, as there is an involvement of cascading effect and higher diffusivity of Cr in Fe as reported by

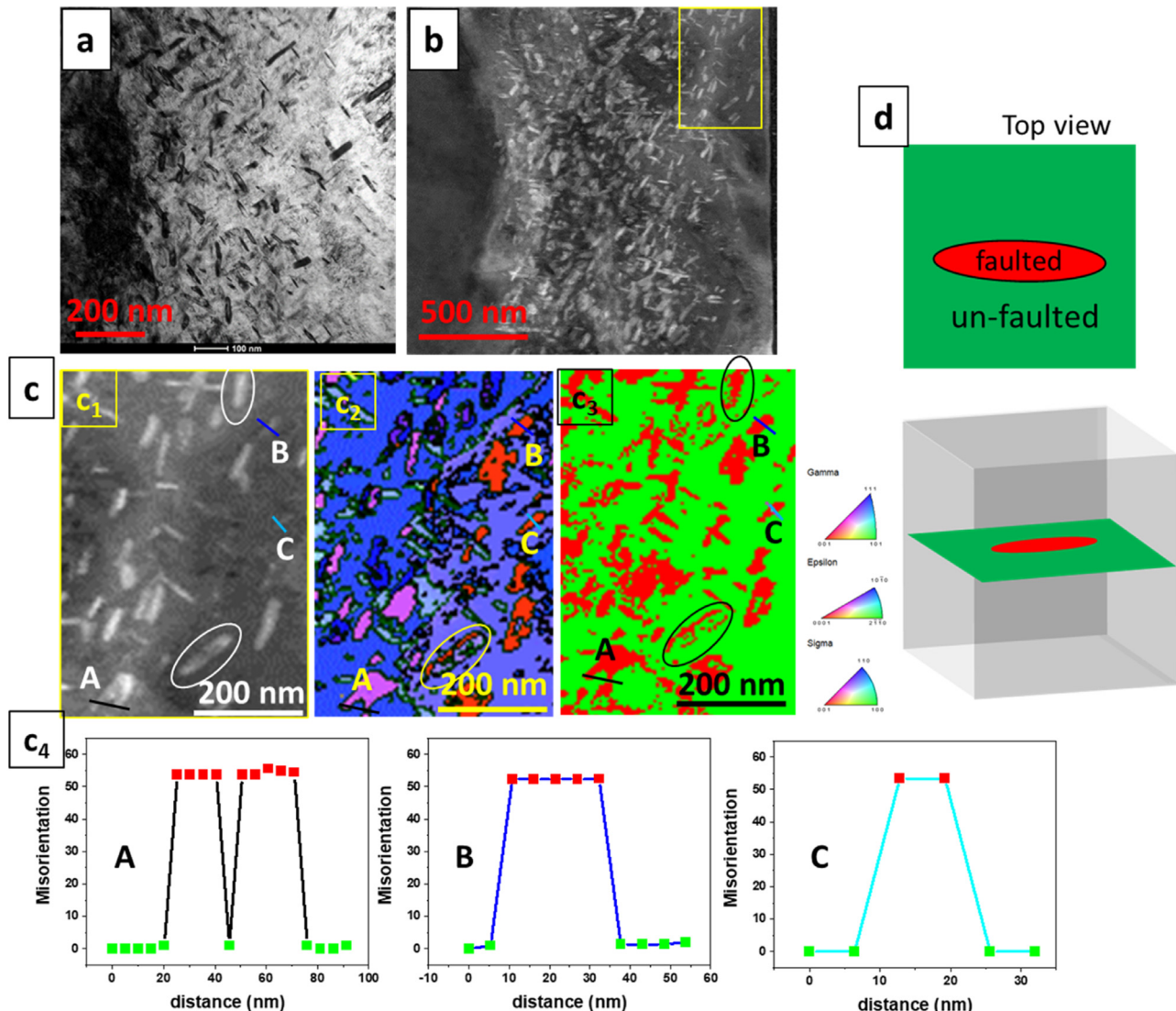


Fig. 8. Exploiting the TRIP effect in HEA to propose the ‘self-healing’ mechanism. 50 dpa/500 °C sample is used to present the results via TEM and PED. (a) micrograph using diffraction contrast presenting large dislocation loops, PED results: (b) low magnification VDF, (c) selected region in (b) taken for PED scan, (c₁) VDF, (c₂) OIM, (c₃) phase map where green is γ -fcc and red is ε -hcp phase. Misorientation plots for regions marked as A, B, and C are shown in c₄, and (d) schematic to show that the faulted loop leads to ε -hcp due to the TRIP effect.

Zhang et al. [57] and He et al. [78]. Temperatures above 600 °C, in general, were shown to lead to σ -bct phase precipitation [62], but the increase in defect density has advanced the process to lower temperatures. Cr depletion from the matrix due to the formation of Cr rich σ -bct precipitates was reported by Babakr et al. [62] to reduce the corrosion resistance of Fe-Cr-Ni alloy. Shi et al. [79] compiled the effect of alloying elements on the corrosion resistance of HEAs. HEAs are reported to have better stress corrosion resistance and a higher repassivation rate in high temperature high-pressure water. Hence, it could be considered a candidate structural material for nuclear applications. Al and Cu are reported in the literature to reduce the corrosion resistance due to the formation of Cr-depleted phases, whereas in a system with Cr-rich σ -bct precipitates, there is Cr depletion in the matrix, again leading to a decrease in corrosion resistance of the alloy. Parakh et al. [80] showed the FCC being a closed packed structure, should have better corrosion resistance than BCC, but it also depends on the elements present that are prone to corrosion. It was also reported that coarser grains improve the corrosion resistance due to less grain boundary area leading to a more open structure with

random atomic arrangement leading to higher diffusivity [81,82]. Again, a similar argument holds for dislocations which are line defects, an array of vacancies. The more the dislocation density, the degraded the corrosion resistance [83].

The elements used in an alloy for nuclear applications should generally have low radioactivity or a faster radiation decay lifetime. Fe and Cr are reported to have reduced activation compared to other elements used in structural applications like Cu, Nb, Ni, Mo, etc. which produce undesirable isotopes when exposed to D-T neutrons [84,85]. Ferritic-Martensitic steels majorly used in nuclear applications increase Cr to about 9–14% and replace elements with lower activation like Mo by W, Nb by Ta, and V [1,84,86]. Gilbert et al. [87] presented the periodic table suggesting a timeline for the elements to be considered as low-level radioactive waste after exposure to 5 years of pulsed operation. From the table and the elements commonly used for HEAs, having Co, Ni, Cu, and Zn increases the decay time to >300–1000 years. Also, as reported in the literature, Co is not advisable for nuclear applications as it will lead to more He and thus He-embrittlement. For this very reason, recent studies are focused on Co-free alloys [23,88–90]. Design

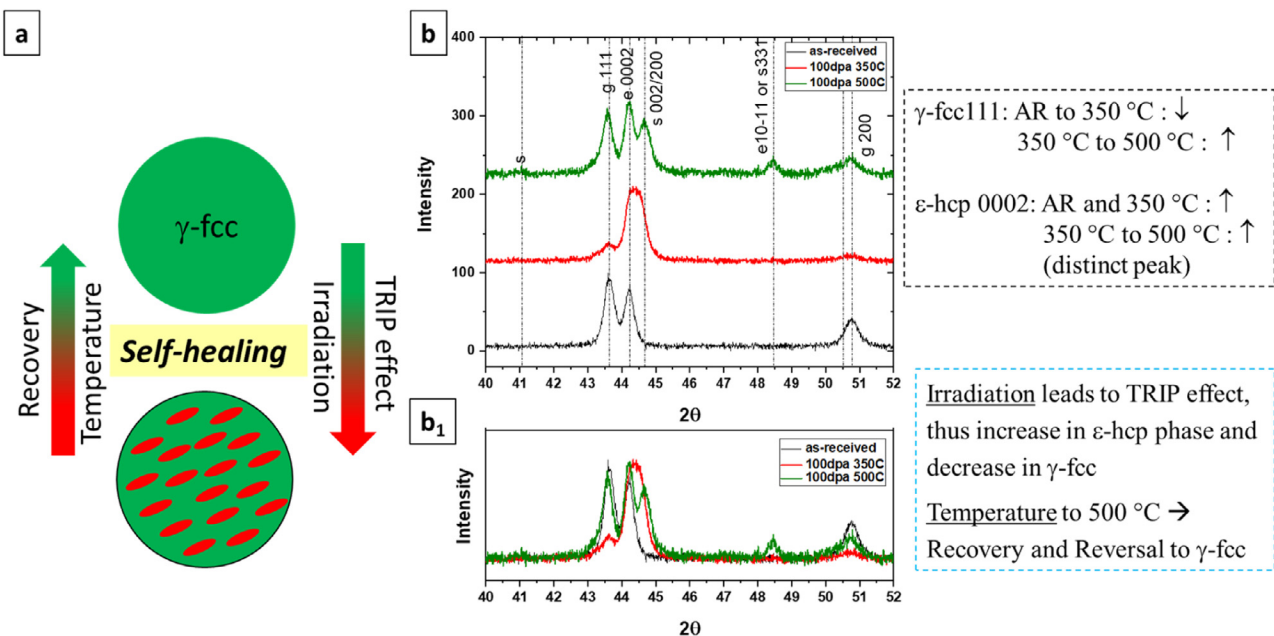


Fig. 9. (a) A schematic proposing the 'self-healing' mechanism in IE TRIP HEA, and (b) selected XRD plots to represent the irradiation and temperature effect leading to TRIP and recovery of IE TRIP HEA.

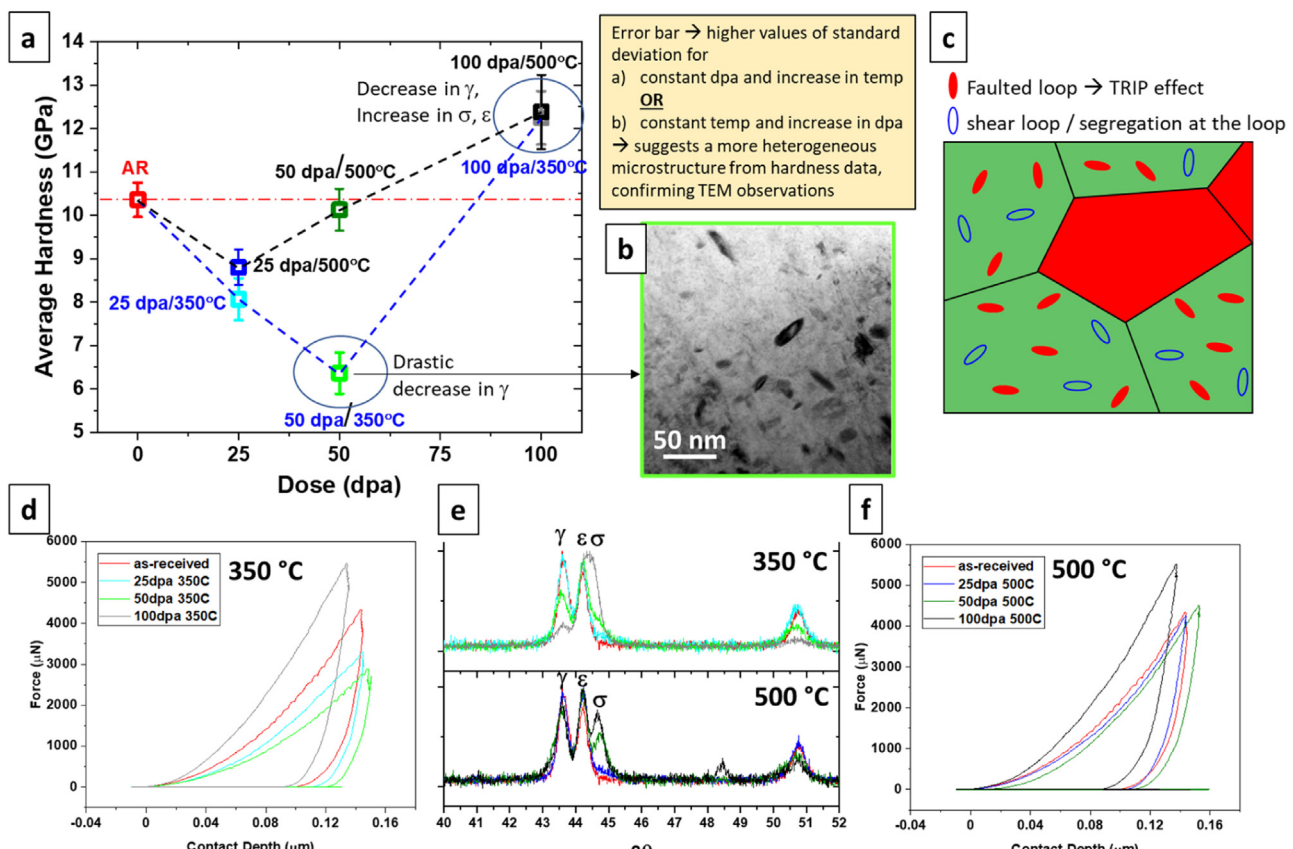


Fig. 10. Mechanical response using nanoindentation. (a) Average hardness plot for different samples, (b) TEM image for 50 dpa 350 °C, exhibiting minimum hardness, (c) schematic for microstructural evolution due to irradiation assisting in reasoning the hardness trends, (d) force vs. depth plots for 350 °C at different dosage levels, (e) intensity vs 2θ results from XRD for all dosages at 350 and 500 °C, and (f) force vs. depth plots for 500 °C at different dosage levels.

of metastability engineered alloys without Co is a good direction based on the current observations.

4. Conclusions

The current work suggests a self-healing mechanism for an inherently radiation tolerant material designed via the innovative engineering technique. A possibility of using deformation induced transformation is suggested to minimize irradiation damage through a self-healing mechanism. This new approach hypothesized and validated a recovery mechanism by counter-balancing radiation induced transformation with temperature induced reverse transformation. This concept of self-healing allows the expansion of the study to other TRIP HEAs and shift of the current dose and temperature envelope to higher values, required for future reactors.

Declaration of Competing Interest

None.

CRediT authorship contribution statement

Priyanka Agrawal: Conceptualization, Data curation, Software, Formal analysis, Writing – original draft. **Sanya Gupta:** Data curation, Writing – review & editing. **Abhijeet Dhal:** Data curation, Writing – review & editing. **Ramprashad Prabhakaran:** Conceptualization, Project administration, Resources, Writing – review & editing. **Lin Shao:** Conceptualization, Project administration, Resources, Writing – review & editing. **Rajiv S. Mishra:** Conceptualization, Project administration, Resources, Supervision, Writing – review & editing.

Data Availability

Data will be made available on request.

Acknowledgement

The authors are grateful to Alden Watts at the University of North Texas (UNT), Denton for preparing the samples and Zhihan Hu at the Department of Nuclear Engineering, Texas A&M University for helping with carrying out the irradiation experiments. The authors would like to acknowledge the Materials Research Facility (MRF) at the UNT, Denton for the microscopy facilities. The authors would also like to thank Stuart Maloy and Dan Edwards (Pacific Northwest National Laboratory) for their suggestions and review of the manuscript.

References

- [1] S.J. Zinkle, L.L. Snead, Designing radiation resistance in materials for fusion energy, *Annu. Rev. Mater. Res.* 44 (2014) 241–267, doi:10.1146/annurev-matsci-070813-113627.
- [2] M. Li, S.J. Zinkle, Physical and mechanical properties of copper and copper alloys, *Compr. Nucl. Mater.* (2012) 667–690 Elsevier Ltd, doi:10.1016/B978-0-08-056033-5.00122-1.
- [3] A. Aitkaliyeva, L. He, H. Wen, B. Miller, X.M. Bai, T. Allen, Irradiation effects in generation IV nuclear reactor materials, *Struct. Mater. Gener. IV Nucl. React.* (2017) 253–283, doi:10.1016/B978-0-08-100906-2.00007-0.
- [4] S.J. Zinkle, K.A. Terrani, L.L. Snead, Motivation for utilizing new high-performance advanced materials in nuclear energy systems, *Curr. Opin. Solid State Mater. Sci.* 20 (2016) 401–410, doi:10.1016/j.cossms.2016.10.004.
- [5] P.J. Maziasz, Developing an austenitic stainless steel for improved performance in advanced fossil power facilities, *JOM* 417 (41) (1989) 14–20 1989, doi:10.1007/BF03220265.
- [6] S.J. Zinkle, P.J. Maziasz, R.E. Stoller, Dose dependence of the microstructural evolution in neutron-irradiated austenitic stainless steel, *J. Nucl. Mater.* 206 (1993) 266–286, doi:10.1016/0022-3115(93)90128-L.
- [7] D.T. Hoelzer, C.P. Massey, S.J. Zinkle, D.C. Crawford, K.A. Terrani, Modern nanosstructured ferritic alloys: a compelling and viable choice for sodium fast reactor fuel cladding applications, *J. Nucl. Mater.* 529 (2020) 151928, doi:10.1016/j.jnucmat.2019.151928.
- [8] Y.R. Lin, W.Y. Chen, L. Tan, D.T. Hoelzer, Z. Yan, C.Y. Hsieh, C.W. Huang, S.J. Zinkle, Bubble formation in helium-implanted nanostructured ferritic alloys at elevated temperatures, *Acta Mater.* 217 (2021) 117165, doi:10.1016/j.actamat.2021.117165.
- [9] C. Sun, S. Zheng, C.C. Wei, Y. Wu, L. Shao, Y. Yang, K.T. Hartwig, S.A. Maloy, S.J. Zinkle, T.R. Allen, H. Wang, X. Zhang, Superior radiation-resistant nano-engineered austenitic 304L stainless steel for applications in extreme radiation environments, *Sci. Rep.* 51 (5) (2015) 1–7 2015, doi:10.1038/srep07801.
- [10] C.P. Massey, D.T. Hoelzer, R.L. Seibert, P.D. Edmondson, A. Kini, B. Gault, K.A. Terrani, S.J. Zinkle, Microstructural evaluation of a Fe-12Cr nanostructured ferritic alloy designed for impurity sequestration, *J. Nucl. Mater.* 522 (2019) 111–122, doi:10.1016/j.jnucmat.2019.05.019.
- [11] C.P. Massey, D.T. Hoelzer, P.D. Edmondson, A. Kini, B. Gault, K.A. Terrani, S.J. Zinkle, Stability of a model Fe-14Cr nanostructured ferritic alloy after long-term thermal creep, *Scr. Mater.* 170 (2019) 134–139, doi:10.1016/j.scriptamat.2019.06.001.
- [12] L. Tan, T. Graening, X. Hu, W. Zhong, Y. Yang, S.J. Zinkle, Y. Katoh, Effects of carbonitrides and carbides on microstructure and properties of castable nanosstructured alloys, *J. Nucl. Mater.* 540 (2020) 152376, doi:10.1016/j.jnucmat.2020.152376.
- [13] B.C. De Cooman, Y. Estrin, S.K. Kim, Twinning-induced plasticity (TWIP) steels, *Acta Mater.* (2018), doi:10.1016/j.actamat.2017.06.046.
- [14] R.S. Mishra, N. Kumar, M. Komarasamy, Lattice strain framework for plastic deformation in complex concentrated alloys including high entropy alloys, *Mater. Sci. Technol.* 31 (2015) 1259–1263, doi:10.1179/1743284715Y.0000000050.
- [15] S. Ranganathan, Alloyed pleasures: multmetallic cocktails, *Curr. Sci.* 85 (2003) 1404–1406.
- [16] D.B. Miracle, O.N. Senkov, A critical review of high entropy alloys and related concepts, *Acta Mater.* 122 (2017) 448–511, doi:10.1016/j.actamat.2016.08.081.
- [17] M.G. Jo, H.J. Kim, M. Kang, P.P. Madakashira, E.S. Park, J.Y. Suh, D.I. Kim, S.T. Hong, H.N. Han, Microstructure and mechanical properties of friction stir welded and laser welded high entropy alloy CrMnFeCoNi, *Met. Mater. Int.* 24 (2018) 73–83, doi:10.1007/s12540-017-7248-x.
- [18] N.A.P.K. Kumar, C. Li, K.J. Leonard, H. Bei, S.J. Zinkle, Microstructural stability and mechanical behavior of FeNiMnCr high entropy alloy under ion irradiation, *Acta Mater.* 113 (2016) 230–244, doi:10.1016/j.actamat.2016.05.007.
- [19] D.S. Aidhy, C. Lu, K. Jin, H. Bei, Y. Zhang, L. Wang, W.J. Weber, Point defect evolution in Ni, NiFe and NiCr alloys from atomistic simulations and irradiation experiments, *Acta Mater.* 99 (2015) 69–76, doi:10.1016/j.actamat.2015.08.007.
- [20] K. Jin, C. Lu, L.M. Wang, J. Qu, W.J. Weber, Y. Zhang, H. Bei, Effects of compositional complexity on the ion-irradiation induced swelling and hardening in Ni-containing equiatomic alloys, *Scr. Mater.* 119 (2016) 65–70, doi:10.1016/j.scriptamat.2016.03.030.
- [21] T. Yang, S. Xia, W. Guo, R. Hu, J.D. Poplawsky, G. Sha, Y. Fang, Z. Yan, C. Wang, C. Li, Y. Zhang, S.J. Zinkle, Y. Wang, Effects of temperature on the irradiation responses of Al_{0.1}CoCrFeNi high entropy alloy, *Scr. Mater.* 144 (2017) 31–35, doi:10.1016/j.scriptamat.2017.09.025.
- [22] C.M. Barr, J.E. Nathaniel, K.A. Unocic, J. Liu, Y. Zhang, Y. Wang, M.L. Taheri, Exploring radiation induced segregation mechanisms at grain boundaries in equiatomic CoCrFeNiMn high entropy alloy under heavy ion irradiation, *Scr. Mater.* 156 (2018) 80–84, doi:10.1016/j.scriptamat.2018.06.041.
- [23] E.J. Pickering, A.W. Carruthers, P.J. Barron, S.C. Middleburgh, D.E.J. Armstrong, A.S. Gandy, High-entropy alloys for advanced nuclear applications, *Entropy* 23 (2021) 98, doi:10.3390/e23010098.
- [24] L. Yang, H. Ge, J. Zhang, T. Xiong, Q. Jin, Y. Zhou, X. Shao, B. Zhang, Z. Zhu, S. Zheng, X. Ma, High He-ion irradiation resistance of CrMnFeCoNi high-entropy alloy revealed by comparison study with Ni and 304SS, *J. Mater. Sci. Technol.* 35 (2019) 300–305, doi:10.1016/J.JMST.2018.09.050.
- [25] T. Yang, S. Xia, W. Guo, R. Hu, J.D. Poplawsky, G. Sha, Y. Fang, Z. Yan, C. Wang, C. Li, Y. Zhang, S.J. Zinkle, Y. Wang, Effects of temperature on the irradiation responses of Al_{0.1}CoCrFeNi high entropy alloy, *Scr. Mater.* 144 (2018) 31–35, doi:10.1016/j.scriptamat.2017.09.025.
- [26] Y. Zong, N. Hashimoto, H. Oka, Study on irradiation effects of refractory bcc high-entropy alloy, *Nucl. Mater. Energy* 31 (2022) 101158, doi:10.1016/J.NME.2022.101158.
- [27] O. El-Atwani, N. Li, M. Li, A. Devaraj, J.K.S. Baldwin, M.M. Schneider, D. Sobieraj, J.S. Wróbel, D. Nguyen-Manh, S.A. Maloy, E. Martinez, Outstanding radiation resistance of tungsten-based high-entropy alloys, *Sci. Adv.* 5 (2019), doi:10.1126/SCIADEVAAV2002.
- [28] S. Xia, M.C. Gao, T. Yang, P.K. Liaw, Y. Zhang, Phase stability and microstructures of high entropy alloys ion irradiated to high doses, *J. Nucl. Mater.* 480 (2016) 100–108, doi:10.1016/j.jnucmat.2016.08.017.
- [29] T. Yang, S. Xia, S. Liu, C. Wang, S. Liu, Y. Fang, Y. Zhang, J. Xue, S. Yan, Y. Wang, Precipitation behavior of Al_xCoCrFeNi high entropy alloys under ion irradiation, *Sci. Rep.* 6 (2016) 1–8 2016 61, doi:10.1038/srep32146.
- [30] S.Q. Xia, X. Yang, T.F. Yang, S. Liu, Y. Zhang, Irradiation Resistance in Al_xCoCrFeNi high entropy alloys, *JOM* 67 (2015) 2340–2344, doi:10.1007/S11837-015-1568-4/FIGURES/7.
- [31] S.S. Nene, M. Frank, P. Agrawal, S. Sinha, K. Liu, S. Shukla, R.S. Mishra, B.A. McWilliams, K.C. Cho, Microstructurally flexible high entropy alloys: linkages between alloy design and deformation behavior, *Mater. Des.* 194 (2020), doi:10.1016/j.matdes.2020.108968.
- [32] S.S. Nene, M. Frank, K. Liu, S. Sinha, R.S. Mishra, B.A. McWilliams, K.C. Cho, Corrosion-resistant high entropy alloy with high strength and ductility, *Scr. Mater.* 166 (2019) 168–172, doi:10.1016/j.scriptamat.2019.03.028.

- [33] M. Frank, Y. Chen, S.S. Nene, S. Sinha, K. Liu, K. An, R.S. Mishra, Investigating the deformation mechanisms of a highly metastable high entropy alloy using in-situ neutron diffraction, *Mater. Today Commun.* 23 (2020) 100858, doi:10.1016/j.mtcomm.2019.100858.
- [34] S. Sinha, S.S. Nene, M. Frank, K. Liu, P. Agrawal, R.S. Mishra, On the evolving nature of c/a ratio in a hexagonal close-packed epsilon martensite phase in transformative high entropy alloys, *Sci. Rep.* 9 (2019) 1–14, doi:10.1038/s41598-019-49904-5.
- [35] K. Liu, S.S. Nene, M. Frank, S. Sinha, R.S. Mishra, Extremely high fatigue resistance in an ultrafine grained high entropy alloy, *Appl. Mater. Today* 15 (2019) 525–530, doi:10.1016/j.apmt.2019.04.001.
- [36] P. Agrawal, S. Shukla, S. Gupta, P. Agrawal, R.S. Mishra, Friction stir gradient alloying: a high-throughput method to explore the influence of V in enabling HCP to BCC transformation in a γ -FCC dominated high entropy alloy, *Appl. Mater. Today* 21 (2020) 100853, doi:10.1016/j.apmt.2020.100853.
- [37] S. Thapliyal, P. Agrawal, P. Agrawal, S.S. Nene, R.S. Mishra, B.A. McWilliams, K.C. Cho, Segregation engineering of grain boundaries of a metastable Fe-Mn-Co-Cr-Si high entropy alloy with laser-powder bed fusion additive manufacturing, *Acta Mater.* 219 (2021) 117271, doi:10.1016/j.actamat.2021.117271.
- [38] S. Sinha, M. Komarasamy, T. Wang, R.S. Haridas, P. Agrawal, S. Shukla, S. Thapliyal, M. Frank, R.S. Mishra, Notch-tensile behavior of $Al_{0.1}CrFeCoNi$ high entropy alloy, *Mater. Sci. Eng. A* 774 (2020), doi:10.1016/j.msea.2020.138918.
- [39] S.S. Nene, P. Agrawal, M. Frank, A. Watts, S. Shukla, C. Morphew, A. Chesiotti, J.S. Park, R.S. Mishra, Transformative high entropy alloy conquers the strength-ductility paradigm by massive interface strengthening, *Scr. Mater.* 203 (2021) 114070, doi:10.1016/j.scriptamat.2021.114070.
- [40] G.R. Odette, M.J. Alinger, B.D. Wirth, Recent developments in irradiation-resistant steels, 10.1146/Annurev.Matsci.38.06.0407.130315. 38 (2008) 471–503. 10.1146/ANNUREV.MATSL38.060407.130315.
- [41] K.L. Murty, I. Charit, Structural materials for Gen-IV nuclear reactors: challenges and opportunities, *J. Nucl. Mater.* 383 (2008) 189–195, doi:10.1016/j.jnucmat.2008.08.044.
- [42] M. Rieth, M. Schirra, A. Falkenstein, P. Graf, S. Heger, H. Kempe, R. Lindau, H. Zimmermann, EUROFER 97 Tensile, charpy, creep and structural tests (FZK-6911), Germany (2003) https://inis.iaea.org/search/search.aspx?orig_q=RN:35032617.
- [43] R.L. Klueh, J.P. Shingledecker, R.W. Swindeman, D.T. Hoelzer, Oxide dispersion-strengthened steels: a comparison of some commercial and experimental alloys, *J. Nucl. Mater.* 341 (2005) 103–114, doi:10.1016/j.jnucmat.2005.01.017.
- [44] K. Sawada, K. Kimura, F. Abe, et al., Data Sheets on the Elevated-Temperature Properties of 9Cr-1Mo-V-Nb Steel Tubes for Boilers and Heat Exchangers (ASME SA-213/SA-213M Grade T91), 9Cr-1Mo-V-Nb Steel Plates for Boilers and Pressure Vessels (ASME SA-387/SA-387M Grade 91) and 9Cr-1Mo-V-Nb Steel Seamless Pipe for High Temperature Service (ASME SA-335/SA-335M Grade P91). NIMS Creep Data Sheet No. 43A, National Institute for Materials Science (2014), doi:10.11503/nims.1047.
- [45] K. Sawada, K. Kimura, F. Abe, et al., Data Sheets on the Elevated-Temperature Properties of 9Cr-0.5Mo-1.8W-V-Nb Steel Tube for Power Boilers (ASME SA-213/SA-213M Grade T92) and 9Cr-0.5Mo-1.8W-V-Nb Steel Pipe for High Temperature Service (ASME SA-335/SA-335M Grade P92). NIMS Creep Data Sheet No. 48B, National Institute for Materials Science (2018), doi:10.11503/nims.1052.
- [46] M.L. Hamilton, D.S. Gelles, R.J. Lobsinger, G.D. Johnson, W.F. Brown, M.M. Paxton, R.J. Puigh, C.R. Eiholzer, C. Martinez, M.A. Blotter, Fabrication Technological Development of the Oxide Dispersion Strengthened Alloy MA957 For Fast Reactor Applications, Pacific Northwest National Laboratory (U.S.), Richland, WA (United States), 2000, doi:10.2172/965199.
- [47] A. Alamo, V. Lambard, X. Avery, M.H. Mathon, Assessment of ODS-14%Cr ferritic alloy for high temperature applications, *J. Nucl. Mater. N. Holl.* (2004) 333–337, doi:10.1016/j.jnucmat.2004.05.004.
- [48] M.J. Alinger, G.R. Odette, G.E. Lucas, Tensile and fracture toughness properties of MA957: implications to the development of nanocomposite ferritic alloys, *J. Nucl. Mater.* 307–311 (2002) 484–489, doi:10.1016/S0022-3115(02)01220-5.
- [49] D. Nakhaie, M.H. Moayed, Pitting corrosion of cold rolled solution treated 17-4 PH stainless steel, *Corros. Sci.* 80 (2014) 290–298, doi:10.1016/j.corsci.2013.11.039.
- [50] H. Luo, H. Su, C. Dong, K. Xiao, X. Li, Electrochemical and passivation behavior investigation of ferritic stainless steel in alkaline environment, *Constr. Build. Mater.* 96 (2015) 502–507, doi:10.1016/j.conbuildmat.2015.08.052.
- [51] R.B. Soares, V. de F.C. Lins, Corrosion resistance of rolled and rerolled super martensitic steel in media containing chlorides and hydrogen sulfide, *Materia (Rio Janeiro)* 22 (2017), doi:10.1590/1517-707620170004.0232.
- [52] J.G. Gigax, E. Aydogan, T. Chen, D. Chen, L. Shao, Y. Wu, W.Y. Lo, Y. Yang, F.A. Garner, The influence of ion beam rastering on the swelling of self-ion irradiated pure iron at 450°C, *J. Nucl. Mater.* 465 (2015) 343–348, doi:10.1016/j.jnucmat.2015.05.025.
- [53] S.J. Zinkle, G.S. Was, Materials challenges in nuclear energy, *Acta Mater.* 61 (2013) 735–758, doi:10.1016/j.actamat.2012.11.004.
- [54] J.G. Gigax, H. Kim, E. Aydogan, F.A. Garner, S. Maloy, L. Shao, Beam-contamination-induced compositional alteration and its neutron-atypical consequences in ion simulation of neutron-induced void swelling, *Mater. Res. Lett.* 5 (2017) 478–485, doi:10.1080/21663831.2017.1323808.
- [55] C.D. Hardie, S.G. Roberts, A.J. Bushby, Understanding the effects of ion irradiation using nanoindentation techniques, *J. Nucl. Mater.* 462 (2015) 391–401, doi:10.1016/j.jnucmat.2014.11.066.
- [56] G. Laplanche, S. Berglund, C. Reinhart, A. Kostka, F. Fox, E.P. George, Phase stability and kinetics of σ -phase precipitation in CrMnFeCoNi high-entropy alloys, *Acta Mater.* 161 (2018) 338–351, doi:10.1016/j.actamat.2018.09.040.
- [57] J. Zhang, G.M. Muralikrishna, A. Asabre, Y. Kalchev, J. Müller, B. Butz, S. Hilke, H. Rösner, G. Laplanche, S.V. Divinski, G. Wilde, Tracer diffusion in the σ phase of the CoCrFeMnNi system, *Acta Mater.* 203 (2021) 116498, doi:10.1016/j.actamat.2020.116498.
- [58] M.H. Tsai, H. Yuan, G. Cheng, W. Xu, W.W. Jian, M.H. Chuang, C.C. Juan, A.C. Yeh, S.J. Lin, Y. Zhu, Significant hardening due to the formation of a sigma phase matrix in a high entropy alloy, *Intermetallics* 33 (2013) 81–86, doi:10.1016/j.intermet.2012.09.022.
- [59] K. Liu, M. Komarasamy, B. Gwalani, S. Shukla, R.S. Mishra, Fatigue behavior of ultrafine grained triplex $Al_{0.3}CoCrFeNi$ high entropy alloy, *Scr. Mater.* 158 (2019) 116–120, doi:10.1016/j.scriptamat.2018.08.048.
- [60] R.S. Haridas, P. Agrawal, S. Yadav, P. Agrawal, A. Gumaste, R.S. Mishra, Work hardening in metastable high entropy alloys: a modified five-parameter model, *J. Mater. Res. Technol.* (2022), doi:10.1016/j.jmrt.2022.04.016.
- [61] M. Frank, S.S. Nene, Y. Chen, S. Thapliyal, S. Shukla, K. Liu, S. Sinha, T. Wang, M.J. Frost, K. An, R.S. Mishra, Direct evidence of the stacking fault-mediated strain hardening phenomenon, *Appl. Phys. Lett.* 119 (2021) 081906, doi:10.1063/5.0062153.
- [62] A.M. Babak, A. Al-Ahmari, K. Al-Jumayah, F. Habiby, Sigma Phase Formation and Embrittlement of Cast Iron-Chromium-Nickel (Fe-Cr-Ni) Alloys, Scientific Research Publishing, 2008. <http://www.scirp.org/journal/PaperInformation.aspx?PaperID=20524&#abstract> (accessed July 19, 2021).
- [63] K. Bawane, X. Liu, T. Yao, M. Khafizov, A. French, J.M. Mann, L. Shao, J. Gan, D.H. Hurley, L. He, TEM characterization of dislocation loops in proton irradiated single crystal ThO₂, *J. Nucl. Mater.* 552 (2021) 152998, doi:10.1016/j.jnucmat.2021.152998.
- [64] M. Jenkins, M. Kirk, Characterisation of Radiation Damage by Transmission Electron Microscopy, (2000). 10.1201/9781420034646.
- [65] M.R. He, S. Wang, K. Jin, H. Bei, K. Yasuda, S. Matsumura, K. Higashida, I.M. Robertson, Enhanced damage resistance and novel defect structure of Cr-FeCoNi under in situ electron irradiation, *Scr. Mater.* 125 (2016) 5–9, doi:10.1016/j.scriptamat.2016.07.023.
- [66] K.Y. Yu, D. Bufford, C. Sun, Y. Liu, H. Wang, M.A. Kirk, M. Li, X. Zhang, Removal of stacking-fault tetrahedra by twin boundaries in nanotwinned metals, *Nat. Commun.* 4 (2013) 1–7 2013 41, doi:10.1038/ncomms2382.
- [67] S. qin Xia, Z. Wang, T. fei Yang, Y. Zhang, Irradiation behavior in high entropy alloys, *J. Iron Steel Res. Int.* 22 (2015) 879–884, doi:10.1016/S1006-706X(15)30084-4.
- [68] Y.N. Osetsky, L.K. Béland, R.E. Stoller, Specific features of defect and mass transport in concentrated fcc alloys, *Acta Mater.* 115 (2016) 364–371, doi:10.1016/j.actamat.2016.06.018.
- [69] Y. Zhang, G.M. Stocks, K. Jin, C. Lu, H. Bei, B.C. Sales, L. Wang, L.K. Béland, R.E. Stoller, G.D. Samolyuk, M. Caro, A. Caro, W.J. Weber, Influence of chemical disorder on energy dissipation and defect evolution in concentrated solid solution alloys, *Nat. Commun.* 6 (2015) 1–9, doi:10.1038/ncomms9736.
- [70] S. Zhao, Y. Osetsky, Y. Zhang, Preferential diffusion in concentrated solid solution alloys: NiFe, NiCo and NiCoCr, *Acta Mater.* 128 (2017) 391–399, doi:10.1016/j.actamat.2017.01.056.
- [71] T. Yang, C. Li, S.J. Zinkle, S. Zhao, H. Bei, Y. Zhang, Irradiation responses and defect behavior of single-phase concentrated solid solution alloys, *J. Mater. Res.* 33 (2018) 3077–3091, doi:10.1557/jmr.2018.285.
- [72] S.J. Zinkle, J.T. Busby, Structural materials for fission & fusion energy, *Mater. Today* 12 (2009) 12–19, doi:10.1016/S1369-7021(09)70294-9.
- [73] P. Agrawal, S. Gupta, S. Shukla, S.S. Nene, S. Thapliyal, M.P. Toll, R.S. Mishra, Role of Cu addition in enhancing strength-ductility synergy in transforming high entropy alloy, *Mater. Des.* 215 (2022) 110487, doi:10.1016/j.matdes.2022.110487.
- [74] S. Gupta, P. Agrawal, S.S. Nene, R.S. Mishra, Friction stir welding of γ -fcc dominated metastable high entropy alloy: microstructural evolution and strength, *Scr. Mater.* 204 (2021) 114161, doi:10.1016/j.scriptamat.2021.114161.
- [75] C. Lu, T. Yang, K. Jin, N. Gao, P. Xiu, Y. Zhang, F. Gao, H. Bei, W.J. Weber, K. Sun, Y. Dong, L. Wang, Radiation-induced segregation on defect clusters in single-phase concentrated solid-solution alloys, *Acta Mater.* 127 (2017) 98–107, doi:10.1016/j.actamat.2017.01.019.
- [76] F.A. Garner, M.B. Toloczkowski, B.H. Sencer, Comparison of swelling and irradiation creep behavior of fcc-austenitic and bcc-ferritic/martensitic alloys at high neutron exposure, *J. Nucl. Mater.* 276 (2000) 123–142, doi:10.1016/S0022-3115(99)00225-1.
- [77] S.J. Zinkle, Fusion materials science: overview of challenges and recent progress, *Phys. Plasmas* 12 (2005) 058101, doi:10.1063/1.1880013.
- [78] F. He, Z. Wang, Q. Wu, J. Li, J. Wang, C.T. Liu, Phase separation of metastable CoCrFeNi high entropy alloy at intermediate temperatures, *Scr. Mater.* 126 (2017) 15–19, doi:10.1016/j.scriptamat.2016.08.008.
- [79] Y. Shi, B. Yang, P.K. Liaw, Corrosion-resistant high-entropy alloys: a review, *Metals (Basel)*, 7, 2017, doi:10.3390/met7020043.
- [80] A. Parakh, M. Vaideya, N. Kumar, R. Chetty, B.S. Murty, Effect of crystal structure and grain size on corrosion properties of $AlCoCrFeNi$ high entropy alloy, *J. Alloys Compd.* 863 (2021) 158056, doi:10.1016/j.jallcom.2020.158056.
- [81] K.D. Ralston, N. Birbilis, Effect of grain size on corrosion: a review, *Corrosion* 66 (2010) 0750051–07500513, doi:10.5006/1.3462912.
- [82] W.R. Osório, C.M. Freire, A. Garcia, The role of macrostructural morphology and grain size on the corrosion resistance of Zn and Al castings, *Mater. Sci. Eng. A* 402 (2005) 22–32, doi:10.1016/j.msea.2005.02.094.
- [83] G.B. Hamu, D. Eliezer, L. Wagner, The relation between severe plastic deforma-

- tion microstructure and corrosion behavior of AZ31 magnesium alloy, *J. Alloys Compd.* 468 (2009) 222–229, doi:[10.1016/j.jallcom.2008.01.084](https://doi.org/10.1016/j.jallcom.2008.01.084).
- [84] E.T. Cheng, Concentration limits of natural elements in low activation fusion materials, *J. Nucl. Mater.* 258–263 (1998) 1767–1772, doi:[10.1016/S0022-3115\(98\)00134-2](https://doi.org/10.1016/S0022-3115(98)00134-2).
- [85] S.J. Piet, E.T. Cheng, S. Fetter, J.S. Herring, Initial integration of accident safety, waste management, recycling, effluent, and maintenance considerations for low-activation materials, *Fusion Technol.* 19 (1991) 146–161, doi:[10.13182/FST19-1-146](https://doi.org/10.13182/FST19-1-146).
- [86] P.J. Barron, A.W. Carruthers, J.W. Fellowes, N.G. Jones, H. Dawson, E.J. Pickering, Towards V-based high-entropy alloys for nuclear fusion applications, *Scr. Mater.* 176 (2020) 12–16, doi:[10.1016/j.scriptamat.2019.09.028](https://doi.org/10.1016/j.scriptamat.2019.09.028).
- [87] M.R. Gilbert, T. Eade, T. Rey, R. Vale, C. Bachmann, U. Fischer, N.P. Taylor, Waste implications from minor impurities in European DEMO materials, *Nucl. Fusion* 59 (2019) 076015, doi:[10.1088/1741-4326/ab154e](https://doi.org/10.1088/1741-4326/ab154e).
- [88] C. Li, X. Hu, T. Yang, N.K. Kumar, B.D. Wirth, S.J. Zinkle, Neutron irradiation response of a Co-free high entropy alloy, *J. Nucl. Mater.* 527 (2019) 151838, doi:[10.1016/j.jnucmat.2019.151838](https://doi.org/10.1016/j.jnucmat.2019.151838).
- [89] A. Karez, J.C. Waite, B. Li, A. Couet, D.E.J. Armstrong, A.J. Wilkinson, Short communication: ‘Low activation, refractory, high entropy alloys for nuclear applications’, *J. Nucl. Mater.* 526 (2019) 151744, doi:[10.1016/j.jnucmat.2019.151744](https://doi.org/10.1016/j.jnucmat.2019.151744).
- [90] D.J. Bowden, *Assessment of Cobalt-free hardfacing Stainless Steel Alloys For Nuclear Applications*, The University of Manchester (United Kingdom, 2017).